

Evolution of QPO during Rising Phase of Discovery Outburst of Swift J1727.8-1613: Estimation of Mass from Spectro-Temporal Study

DIPAK DEBNATH,¹ HSIANG-KUANG CHANG,^{1,2} SUJOY KUMAR NATH,^{1,3} AND LEV TITARCHUK⁴

¹*Institute of Astronomy, National Tsing Hua University, Hsinchu 300044, Taiwan*

²*Department of Physics, National Tsing Hua University, Hsinchu 300044, Taiwan*

³*Indian Center for Space Physics, 466 Barakhola, Netai Nagar, Kolkata 700099, India*

⁴*Dipartimento di Fisica, University di Ferrara, Via Saragat 1, I-44122 Ferrara, Italy*

Submitted to ApJ

ABSTRACT

The rising phase of the 2023–24 outburst of the recently discovered bright transient black hole candidate Swift J1727.8-1613 was monitored by *Insight*-HXMT. We study the evolution of hard (4–150 keV) and soft (2–4 keV) band photon count rates, the hardness ratio (HR), and QPO frequencies using daily observations from the HXMT/LE, ME, and HE instruments between August 25 and October 5, 2023. The QPO frequency is found to be strongly correlated with the soft-band X-ray count rates, and spectral photon indices. In contrast, a strong anti-correlation is observed between HR and QPO frequency, as well as between HR and photon index. Based on the evolution of the QPO frequency, the rising phase of the outburst is subdivided into six parts, with parts 1–5 fitted using the propagating oscillatory shock (POS) solution to understand the nature of the evolution from a physical perspective. The best-fitted POS model is obtained with a black hole mass of $13.34 \pm 0.02 M_{\odot}$. An inward-propagating shock with weakening strength (except in part 4) is observed during the period of our study. The POS model-fitted mass of the source is further confirmed using the QPO frequency (ν)-photon index (Γ) scaling method. From this method, the estimated probable mass of Swift J1727.8-1613 is obtained to be $13.54 \pm 1.87 M_{\odot}$.

Keywords: X-ray binary stars(1811) – X-ray transient sources(1852) – Black holes(162) – Black hole physics(159) – Accretion(14) – Shocks (2086)

1. INTRODUCTION

Stellar-mass black holes, especially transient black hole candidates (BHCs), are fascinating objects in X-rays as they exhibit rapid evolution of timing and spectral properties during their active (i.e. outbursting) phases. Various temporal and spectral features, along with their evolution, are generally observable during the outbursts of transient BHCs. These timing and spectral properties, including quasi-periodic oscillations (QPOs), jets, and outflows, are found to be strongly correlated with each other (see Remillard & McClintock 2006; Belloni et al. 2005; Nandi et al. 2012; Debnath et al. 2015, 2021; Jana et al. 2017). During a classical or type-I outburst of a transient BHC, four distinct spectral states are typically observed: hard (HS), hard-intermediate (HIMS), soft-intermediate (SIMS), and

soft (SS). These states form a hysteresis loop in the following sequence: HS \rightarrow HIMS \rightarrow SIMS \rightarrow SS \rightarrow SIMS \rightarrow HIMS \rightarrow HS. However, in a ‘failed’ or type-II outburst, softer states (and sometimes even intermediate states) are found to be missing (see Debnath et al. 2017, and references therein).

Although there is ongoing debate about what triggers an outburst in a transient BHC, it is generally believed that an outburst is initiated by a sudden enhancement of viscosity at the outer edge of the disk (Ebisawa et al. 1996). Recently, Chakrabarti et al. (2019) proposed that matter supplied by the companion accumulates at the pile-up radius (X_p), located at a far distance between the black hole and the Lagrange point L1. During the quiescence phase, the accumulation of a large amount of matter at X_p increases viscosity and instability. When viscosity crosses a critical threshold, it triggers the onset of a new outburst. In a type-I outburst, all accumulated matter at X_p is cleared, whereas in a type-II outburst, matter is only partially cleared, leaving behind residual material that is eventually expelled dur-

ing the next type-I outburst along with freshly accumulated matter (Chakrabarti et al. 2019; Bhowmick et al. 2021; Chatterjee et al. 2022). Recently, Russell et al. (2018) developed a X-ray Binary New Early Warning System (XB-NEWS) for the possible outburst of a transient BHC by monitoring its increasing optical activity in the quiescence phase.

Low-frequency (0.01–30 Hz) quasi-periodic oscillations (LFQPOs) are commonly observed during the hard and intermediate spectral states of transient black hole candidates (BHCs). QPOs appear as peaks in the Fourier-transformed power-density spectra (PDS) of light curves, characterized by narrow noise components, and arise due to rapid variability in X-ray intensities. They provide crucial insights into the dynamics of accretion flows around black holes. Based on their properties (centroid frequency, Q-value, rms amplitude, noise, lag, etc.), LFQPOs are classified into three types: A, B, and C (Casella et al. 2005). Generally, the primary frequency of type-C QPOs evolves monotonically during the HS and HIMS of both the rising and declining phases of an outburst. In contrast, type-B and type-A QPOs are sporadically observed in the SIMS.

Several models have been proposed to explain the origin of LFQPOs. The Lense-Thirring precession model (Stella & Vietri 1999) suggests that LFQPOs arise due to the precession of a tilted inner accretion flow caused by frame-dragging effects near the black hole. The precessing hot flow model (Ingram & Done 2011) proposes that a truncated disk, along with an inner hot flow, undergoes slow, global precession, modulating X-ray emissions. The accretion-ejection instability model (Tagger & Pellat 1999; Rodriguez et al. 2002) suggests that LFQPOs result from magnetohydrodynamic instabilities in magnetized accretion disks. Titarchuk et al. (1998) associated QPOs with viscous magneto-acoustic resonance oscillations in the transition layer surrounding the Compton cloud. Trudolyubov et al. (1999) attributed LFQPOs to perturbations within a Keplerian disk, while Titarchuk & Osheroich (2000) explained them as global disk oscillations or oscillations of a warped disk. According to the shock oscillation model (SOM) developed by Chakrabarti and collaborators (Molteni et al. 1996; Ryu et al. 1997), LFQPOs originate from shock oscillations in the accretion flow. In the Two-Component Advective Flow (TCAF) solution (Chakrabarti & Titarchuk 1995), a hot Comptonizing region, known as ‘CENBOL’, naturally forms in the post-shock region. In the SOM framework, shock oscillations occur due to the heating and cooling effects within the CENBOL. The model suggests that sharp type-C QPOs arise from resonance oscillations of the shock, while type-B QPOs occur either due to the non-satisfaction of the Rankine-Hugoniot condition (necessary for stable shock formation) or due to a weakly resonating Compton cloud. Broader type-A QPOs are attributed to weak oscillations of the shockless centrifu-

gal barrier (see, Chakrabarti et al. 2015). To explain evolution of QPO frequencies during rising and declining phases of transient BHCs a time varying form of the SOM namely propagating oscillatory shock (POS) model was introduced by Chakrabarti and his collaborators in 2005 (see, Chakrabarti et al. 2005, 2008).

In astronomical sources, particularly in compact objects, mass is a crucial intrinsic parameter. Accurately determining the mass of the central black hole in a binary system is essential for understanding accretion-ejection processes. However, direct dynamical measurements of black hole mass are sometimes not possible due to the absence of detectable binary companion information (e.g., if the companion is too faint or non-detectable). In such cases, alternative methods are employed, including: QPO frequency (ν)–photon index (Γ) correlation method (Shaposhnikov & Titarchuk 2007, 2009); High-frequency QPO (HFQPO)–spin (a) correlation method (Motta et al. 2014); Inverse scaling relation with observed HFQPOs (Remillard & McClintock 2006); QPO frequency evolution method (Iyer et al. 2015); TCAF model-based spectral fitting method (Molla et al. 2016). The spin and inverse scaling methods are not universally applicable, as HFQPOs are rare phenomena observed in only a limited number of BHCs. However, the ν – Γ correlation method has been widely used to estimate the masses of stellar-mass black holes, active galactic nuclei (AGNs), and neutron star systems. The TCAF model-based spectral fitting method has also been applied to estimate the probable masses of many transient BHCs.

Observationally, the spectral index increases as black holes transit from hard to intermediate to soft states. During the rising phase of transient BHCs, as the spectral state evolves from HS to HIMS, QPO frequencies exhibit a monotonic increase. Conversely, during the declining phase, as the source transits from HIMS to HS, QPO frequencies show a monotonic decrease. According to the TCAF model, during the rising phase of an outburst, an increasing rate of Keplerian matter (the source of thermal photons) pushes the shock inward, causing the Compton cloud to shrink. The enhanced supply of Keplerian matter increases cooling, reducing the proportion of hard photons and making the spectrum softer, thereby increasing the spectral index. Since QPO frequency follows an inverse relation with the shock location (X_s), i.e., $\nu \sim X_s^{-3/2}$, this results in a monotonic rise in QPO frequency. During the declining phase, the shock moves outward due to a rapidly decreasing supply of Keplerian matter, leading to a relative increase in the dominance of hard photons. As a result, QPO frequencies decrease while the spectrum hardens. In the SIMS, both spectral index and observed QPO frequencies are generally found within narrow ranges (see Nandi et al. 2012). Titarchuk et al. (1998) proposed that the spectral index is a fundamental property of the corona,

implying a direct correlation between the spectral index and QPO frequency. They also suggested that QPO frequency scales inversely with black hole mass, following the relation $\nu \sim M^{-1}$. Observationally, stellar-mass black holes ($M_{\text{BH}} \sim 10M_{\odot}$) exhibit LFQPOs in the 0.1–30 Hz range and HFQPOs in the kHz range, while supermassive black holes ($M_{\text{BH}} \sim 10^6\text{--}10^9M_{\odot}$) exhibit LFQPOs in the mHz– μ Hz range.

The Galactic transient BHC Swift J1727.8-1613 was discovered by Swift/BAT as a Gamma-Ray Burst candidate (GRB 230824A) on August 24, 2023 (Kennea & Swift Team 2023). This bright outburst (maximum flux ~ 7.6 Crab) lasted for approximately nine months and was extensively studied across multiple wavelengths. The detection of its companion and radial velocity curve through spectro-photometric studies led to the dynamical confirmation of the source as a black hole by Sánchez et al. (2025). They estimated an orbital period of $P_{\text{orb}} = 10.81 \pm 0.001$ h and lower mass limit of the BH as $3.12 \pm 0.10 M_{\odot}$. Peng et al. (2024) estimated the spin ($a \sim 0.98$) and inclination angle ($i \sim 40^\circ$) of the source. However, Debnath et al. (2024) classified Swift J1727.8-1613 as a high-inclination BHC ($i \sim 85^\circ$), which aligns with the detection of soft time lags. The energy-averaged polarization degree ($4.1\% \pm 0.2\%$) and polarization angle ($2.2^\circ \pm 1.3^\circ$) were measured by Veledina et al. (2023). Polarization studies were also conducted by Podgorný et al. (2024) and Ingram et al. (2024). LFQPOs have been detected in both soft and hard X-ray bands (Debnath et al. 2024; Mereminskiy et al. 2024; Nand et al. 2024; Zhu & Wang 2024).

In this study, we analyze the evolution of LFQPOs during the rising phase of the 2023-24 outburst of Swift J1727.8-1613 using Insight-HXMT data. By studying QPO evolution with the propagating oscillatory shock (POS) model and the ν – Γ correlation method, we estimate the mass of the source. The paper is organized as follows: §2 provides a summary of the POS model and ν – Γ correlation method. The §3 describes observations, data reduction, and analysis procedures. In §4, we present the results, while §5 discusses our findings and presents the conclusions.

2. MODELS FOR DATA ANALYSIS

2.1. Propagating Oscillatory Shock (POS) Model

Chakrabarti (1990) showed that, due to the satisfaction of the Rankine-Hugoniot conditions, unique standing shocks may form in the presence of a strong centrifugal barrier, where infalling energy may be dissipated, leading to the formation of jets and outflows. At the shock location (X_s), matter that was flowing supersonically becomes subsonic and piles up in the post-shock region. This post-shock region, namely CENBOL, acts as the hot corona, up-scattering soft photons via inverse Comptonization. It may also oscillate if its cooling timescale roughly matches the infall time in this region (Molteni et al. 1996). Due to the non-satisfaction of

the Rankine-Hugoniot conditions, the shock may also oscillate (Ryu et al. 1997). Chakrabarti et al. (2015) observationally showed that resonance shock oscillation occurs only when the ratio between the Compton cooling time and the infall time falls within approximately 50% of unity, i.e., between 0.5 and 1.5.

We observe variations in hard X-ray fluxes as the shock oscillates, i.e., as the size of the hot Compton cloud changes. During the oscillation phase, when the shock moves inward (due to an increase in the cooling rate with the rise in thermal seed photons from the Keplerian disk), the size of the Compton cloud shrinks. This reduces the interception of thermal photons as well as the number of emitted hard photons from Compton cloud or CENBOL. Similarly, when the shock moves outward (due to a faster decrease in the Keplerian disk accretion rate relative to the sub-Keplerian halo rate), the size of the Compton cloud increases, allowing more thermal photons to interact. This, in turn, increases the number of up-scattered hard photons from CENBOL. Overall, variations in the number of hard photons during the shock oscillation phases are reflected in the light curve, showing QPO-like features in the power density spectrum (PDS).

As the supply from the Keplerian disk and the sub-Keplerian halo varies during the outbursting phases, we generally observe the evolution of QPOs during both the rising and declining phases of an outburst. During the rising phase, the oscillating shock is found to move inward as the Keplerian disk accretion rate increases over time. Since the QPO frequency (ν_{QPO}) is found to be inversely proportional to the infall timescale ($t_{\text{infall}} \sim RX_s(X_s - 1)^{1/2}$, where $R(= \rho_+/\rho_-)$ is the shock compression ratio, i.e., the ratio between post-shock and pre-shock densities and X_s is the shock location), we observe a monotonically increasing QPO frequency during the rising phase of an outburst. Similarly, during the declining phase of the outburst, an opposite trend is generally observed, as the shock is found to recede.

In Chakrabarti et al. (2005, 2008), a modified time-varying shock oscillation model, i.e., the propagating oscillatory shock (POS) model, was proposed to study the evolution of monotonically evolving QPO frequencies during the rising and declining phases of the 2005 outburst of the Galactic transient BHC GRO J1655-40. According to this model, the frequency of the QPO (ν_{QPO}) depends on the location (X_s) and strength ($\beta_s = 1/R$) of the shock, as well as on the mass of the black hole.

Thus, the instantaneous QPO frequency ν_{QPO} (in s^{-1}) is given by

$$\nu_{\text{QPO}} = \frac{\nu_{s0}}{t_{\text{infall}}} = \frac{c^3}{2GM_{\text{BH}}[RX_s(X_s - 1)^{1/2}]}, \quad (1)$$

where $\nu_{s0} = c/r_s = c^3/2GM_{\text{BH}} = 10^5/(M_{\text{BH}}/M_{\odot})$ is the inverse of the light crossing time of a black hole of

mass M_{BH} in s^{-1} and c is the velocity of light, $r_s = 2GM_{BH}/c^2$ is the Schwarzschild radius.

In the drifting or evolving shock scenario, $X_s = X_s(t)$ is time-dependent and can be expressed as

$$X_s(t) = X_{s0} \pm \frac{v(t)t}{r_s}, \quad (2)$$

where ‘-’ sign is used for inward and ‘+’ sign is used for receding shock motion. The shock velocity $v(t)$ may be accelerating, decelerating or constant and can be written as

$$v(t) = v_0 \pm v_a t, \quad (3)$$

where v_0 is the initial shock velocity and v_a is the velocity acceleration (‘+’)/deceleration (‘-’) term.

Generally during the rising phase of an outburst, the shock strength becomes weaker as the R decreases. On the day of the highest evolving QPO, it becomes even weaker, approaching $R \sim 1$. The value of R generally follows the equation

$$\beta_s = \frac{1}{R} = \frac{1}{R_0} + \alpha t_d^2, \quad (4)$$

where R_0 is the initial compression ratio, α is the controlling factor of the reduction of the shock strength over time (t_d).

2.2. QPO Frequency (ν) - Photon Index (Γ) Correlation Scaling

It is well established that the power-law photon index has a direct correlation with the properties of the Compton cloud or corona in black holes. The emitted hard X-ray fluxes are also found to be correlated with the size of the corona. This, in turn, affects the frequency of the observed QPOs. Titarchuk & Fiorito (2004) introduced a model to study correlations between the observed QPO frequency (ν) and the model-fitted spectral photon index (Γ). Using a known source as a reference, this method is employed to estimate the masses of various compact objects, including stellar-mass BHs, AGNs, neutron stars, etc. (see Shaposhnikov & Titarchuk 2007, 2009). In this model, the central source is considered to be surrounded by a ‘‘Compton cloud’’ along with a transition layer between this Compton cloud and the Keplerian disk. According to this model, the origin of the QPO frequencies is explained as the magneto-acoustic resonance oscillation frequency of the bounded transition layer (Titarchuk & Wood 2002), while the spectral photon index is attributed to changes in the size of the Compton cloud.

When studying the correlation between the QPO frequency and the photon index, it is generally observed that, before saturating at a certain value, the photon index initially exhibits an increasing trend with the QPOs. Thus, there are two primary phases: a trending phase and a constant phase, separated by the transition frequency (ν_{tr}).

The empirical relation given by Shaposhnikov & Titarchuk (2007) is

$$\Gamma(\nu) = A - D B \ln \left[\exp \left(\frac{\nu_{tr} - \nu}{D} \right) + 1 \right], \quad (5)$$

where A represents the saturation level of the photon index, B scales with the mass of the BH (M_{BH}) and the transition/threshold frequency above which the photon index saturates. The parameter D controls the transition, i.e., how quickly the saturation is reached.

In Shaposhnikov & Titarchuk (2009), a more generalized version of this function is provided, making it applicable for estimating the mass and distance of an unknown compact object from the correlations of $\nu - \Gamma$, or $\nu - N_{bmc}$ (where N_{bmc} is the bulk motion Comptonization model-fitted spectral normalization):

$$f(x) = A - D B \ln \left[\exp \left(\frac{1 - (x/x_{tr})^\beta}{D} \right) + 1 \right], \quad (6)$$

where x is ν and $f(x)$ is either Γ or N_{bmc} .

Using Eqs. (5) and (6), one can fit the variation of the QPOs with Γ or N_{bmc} and extract a set of parameters: A , B , D , ν_{tr} or x_{tr} , β (only from Eq. 6).

To estimate mass of an unknown source, $\nu - \Gamma$ variations are fitted using Eq. (6) for both unknown and known reference sources. According to Shaposhnikov & Titarchuk (2009), the scaling relation for the mass estimation is given by

$$M_U = \left(\frac{\nu_{trU}}{\nu_{trR}} \right) \times M_R, \quad (7)$$

where suffixes U , R mark unknown and known reference sources respectively. The ratio between transition frequencies, i.e., $s_\nu = \frac{\nu_{trU}}{\nu_{trR}}$ acts as a scaling factor to estimate the mass of the unknown source.

3. OBSERVATION AND DATA ANALYSIS

We study archival data of 51 observations across all three energy band payloads (LE, ME, HE) of the *Insight-HXMT* starting from its first day of observation. One observation per day is used, except on 2023 Sep 13, where eight observations are taken. The dataset spans from 2023 Aug 25 (MJD=60181.42) to 2023 Oct 05 (MJD=60222.20).

To study properties of QPOs, count rates, and hardness-ratios (HRs), we generated 1 s and 0.01 s time binned light curves in four different energy bands: 2 – 4 keV of LE, 4 – 10 keV of LE, 10 – 30 keV of ME, and 30 – 150 keV of HE. For spectral analysis, we used default energy ranges for all three instruments. The data extraction for generating light curves and spectral files was performed using `hpipeline` pipeline within the `HEASoft` software package (v.6.34) from HeaSARC.

To study the variation of the count rates and hardness ratios, we use 1 s time-binned light curves. For power

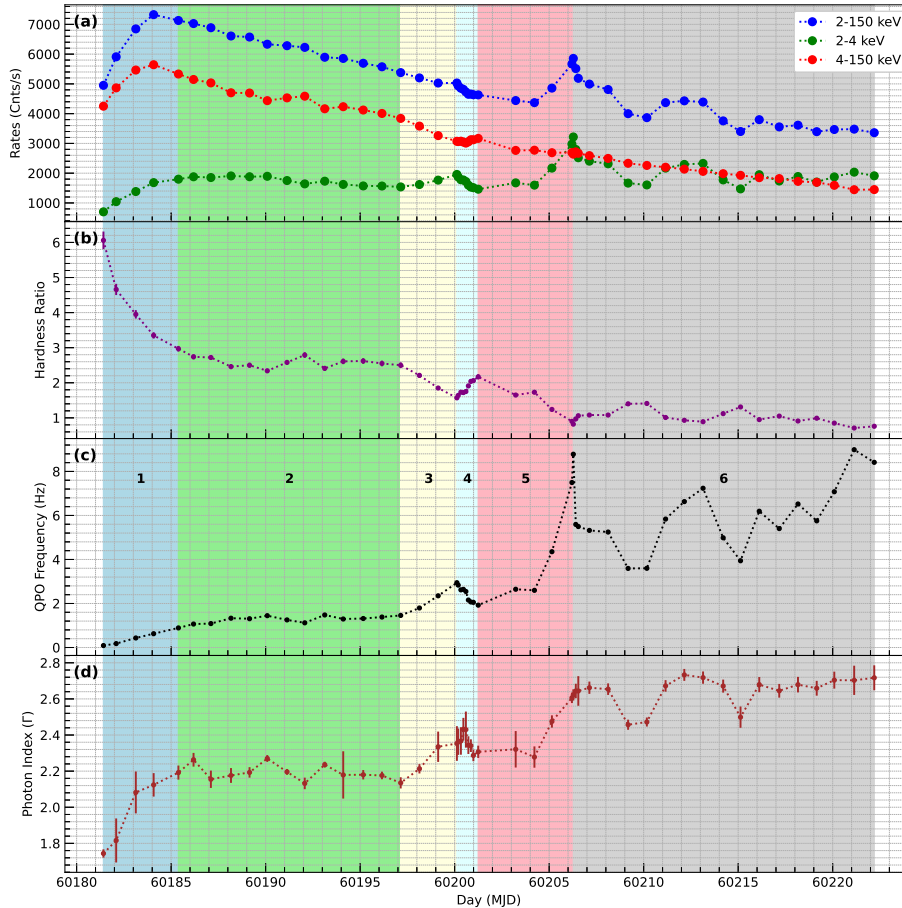


Figure 1. (a) Variation of *Insight*-HXMT rates in soft X-ray (SXR; 2 – 4 keV), hard X-ray (HXR; 4 – 150 keV), and total (TXR; 2 – 150 keV) energy bands shown in the top panel. (b) The middle panel shows the variation in the hardness ratio (HR, i.e., the ratio between HXR and SXR rates). (c) The evolution of the frequency of the observed QPOs is shown in the second lower panel. (d) Variation of photon index are shown bottom panel. Background shades sub-divide evolution of the QPO frequencies into six parts: 1: monotonically rising, 2: roughly constant, 3: monotonically rising, 4: monotonically decreasing, 5: rapidly rising, and 6: sporadically increasing or decreasing. According to the rate variation, parts 1-3 are defined as stage-I, where TXR follows HXR, while in stage-II (parts 4-6), TXR follows SXR.

density spectra (PDS), we use 0.01 s time-binned light curves in the ME energy band. To determine the parameters (centroid frequency, fwhm, power) of the QPOs, the PDS are fitted with the Lorentzian model in the XRONOS package of HEASoft.

The combined HEXTE/LE (2 – 10 keV), ME (10 – 35 keV), and HE (27 – 150 keV) data, covering a broad energy range of 2 – 150 keV, are fitted with `constant × tbabs(diskbb+pexrav)`. A variable hydrogen column density (N_H) in the range of $(0.5 - 3) \times 10^{22}$ atoms cm^{-2} is used for the absorption model `tbabs`. Since a strong reflection feature with a cutoff power-law at higher energies is present throughout the entire rising phase, we use the `pexrav` model (Magdziarz & Zdziarski 1995) to fit the spectra. The best fits are obtained based on the reduced χ^2 statistics (~ 1).

4. RESULTS

4.1. Outburst Profile

We used 1 s time-binned light curves from all three energy band instruments of *Insight*-HXMT to study the outburst profile during the rising phase (MJD=60181.42 - 60222.20) of Swift J1727.8-1613. In Fig. 1(a), we show the variation in the count rates in Soft X-Ray (SXR; 2 – 4 keV), Hard X-Ray (HXR; 4 – 150 keV), and Total X-Ray (TXR; 2 – 150 keV) energy bands.

All three bands showed an initial rise. The evolution of these three rates can be classified into two stages. In stage-I (up to 2023 Sep. 13; MJD=60200.12), TXR and HXR followed a similar trend, whereas in stage-II (from 2023 Sep. 13 to Oct. 05; MJD=60200.12-60222.20), TXR and SXR showed roughly similar variability.

The total and HXR band rates peaked on the 4th day (MJD=60184.07), whereas SXR showed the maximum rate on the 6th day (MJD=60186.19). There is a roughly

Table 1. Correlations Fitted with Scaling Formulae

Set	P_{cor}	SP_{cor}	A	B	x_{tr}	β
SWIFT J1727.8-1613						
$\nu - SXR$	0.688	0.629	--	--	--	--
$\nu - HR^a$	-0.821	-0.997	$0.45^{\pm 0.07}$	$5.57^{\pm 0.53}$	$0.31^{\pm 0.08}$	$0.40^{\pm 0.04}$
$\Gamma - HR^a$	-0.939	-0.956	$0.64^{\pm 0.05}$	$6.82^{\pm 0.90}$	$1.77^{\pm 0.07}$	$3.48^{\pm 0.35}$
$\nu - \Gamma^b$	0.913	0.951	$2.83^{\pm 0.08}$	$0.91^{\pm 0.10}$	$1.31^{\pm 0.14}$	$0.59^{\pm 0.08}$
GRO J1655-40						
$\nu - \Gamma^b$	--	--	$2.21^{\pm 0.01}$	$0.57^{\pm 0.01}$	$2.82^{\pm 0.09}$	$1.82^{\pm 0.09}$

^a Eq. (8) is used for correlations of HR with ν_{QPO} , or Γ .

^b Eq. (6) is used for correlation of ν_{QPO} with Γ .

2.12 day gap between the HXR and SXR band rates. According to Jana et al. (2016), this might indicate an important accretion flow parameter, namely the viscous timescale, which represents how high-viscosity Keplerian disk matter flows during the outburst.

4.2. Hardness-Ratio (HR)

The variation of the hardness ratio (HR) or X-ray color-color ratio is shown in Fig. 1(b). We used the ratio between the broad-band 4 – 150 keV energy HXR count rate (using the combined light curves of all three HXMT instruments) with 2–4 keV band HXMT/LE SXR count rate as HR. A sharp decrease in HR (6.06 – 2.97) is observed within ~ 4 days between 2023 Aug 25-29 (MJD = 60181.42-60185.38). Then, HR remains nearly constant around 2.5 for the next ~ 12 days until 2023 Sep 10 (MJD = 60197.15). Subsequently, HR shows a decreasing trend (2.50 – 1.57) for the next ~ 3 days until 2023 Sep 13 (MJD = 60200.12).

After that, a sharp rise in HR (1.57 – 2.17) is observed over the next ~ 1.3 days until 2023 Sep 14 (MJD = 60201.25). Then, a decreasing trend in HR (2.17 – 0.82) is found over ~ 5 days until 2023 Sep 19 (MJD = 60206.28). After that, HR is observed to fluctuate within a wide range of 0.71 – 1.41 until the last day of our observation (MJD = 60222.20).

4.3. Low frequency QPOs

A strong signature of sharp type-C QPOs is observed throughout the entire observation period. The evolution of the frequency of the primary QPOs is shown in Fig. 1(c). Based on the variation in QPOs, we classified the rising phase of the outburst into six parts. In these parts, the QPO frequency exhibits the following trends: *i*) monotonically rising (MJD = 60181.42-60185.38 with ν_{QPO} in the range 0.09 – 0.89 Hz), *ii*) roughly constant (MJD = 60185.38-60197.15 with ν_{QPO} in the range 1.07 – 1.46 Hz), *iii*) monotonically rising (MJD = 60197.15-60200.12 with ν_{QPO} in the range 1.46 – 2.94 Hz), *iv*) monotonically decreasing (MJD = 60200.12-60201.25 with ν_{QPO} in the range 2.94 – 1.92 Hz), *v*) rapidly rising (MJD = 60201.25-

60206.28 with ν_{QPO} in the range 1.92 – 8.78 Hz), and *vi*) sporadically increasing or decreasing (MJD = 60206.28-60222.20 with ν_{QPO} in the range 3.94 – 8.99 Hz).

Parts 1-5 are defined as the evolving phase, during which the frequency of the observed QPOs evolves from 0.09 Hz (on 2023 Aug 25; MJD = 60181.42) to 8.78 Hz (on 2023 Sep 19; MJD = 60206.28). We further studied this evolving phase of the QPOs using the propagating oscillatory shock (POS) solution to understand the nature of the evolution from a physical perspective. Part 6 is defined as a non-evolving or sporadic phase since no clear trend is observed.

4.4. Correlation of QPO frequency with SXR and Photon Index

It is quite evident from Fig. 1 that the evolution of the QPO frequency follows a trend roughly similar to that of the soft X-ray rate (SXR) in the 2 – 4 keV HEXTE/LE band. To confirm this statistically, we studied the correlation between ν_{QPO} and SXR using Pearson and Spearman rank correlation methods (see Fig. 2a). Both methods indicate the existence of a strong positive correlation. The Pearson correlation yields a correlation coefficient of $P_{cor} = 0.688$ with a p-value of 2.4×10^{-8} . The Spearman rank correlation gives a correlation coefficient of $SR_{cor} = 0.629$ with a p-value of 7.8×10^{-7} .

The variation of the *peaxrav* model-fitted photon index (Γ) exhibits a trend roughly similar to that of ν_{QPO} , except during the late rising phase (see Fig. 1d). Pearson and Spearman rank correlation analyses were performed on the variation of ν_{QPO} vs. Γ (see Fig. 2b). The correlation coefficients from Pearson ($P_{cor} = 0.913$ with a p-value of 9.2×10^{-21}) and Spearman rank ($SR_{cor} = 0.951$ with a p-value of 1.4×10^{-26}) suggest a strong positive correlation between ν_{QPO} and Γ . Furthermore, this correlation is fitted using the scaling formula of Eq. (6) (for more details, see §4.7 & Table 1). In Fig. 2b, the ν_{QPO} - Γ data points (red) along with the model-fitted curve (solid black) are shown.

4.5. Anti-correlation of HR with QPO frequency and Photon Index

The hardness ratio (HR) exhibits a trend opposite to that of the QPO frequency (see Fig. 1). From a simple observation, this feature appears to be more prominent during the evolving phase of the QPO frequency (parts 1-5). To confirm this statistically, we analyzed the Pearson and Spearman rank correlations. Both correlation methods indicate a strong negative or anti-correlation between the QPO frequency and HR (see Fig. 2c). The Pearson correlation yields a correlation coefficient of $P_{cor} = -0.821$ with a p-value of 1.6×10^{-13} . The Spearman rank correlation gives a correlation coefficient of $SR_{cor} = -0.997$ with a p-value of 1.3×10^{-55} .

The trend between the QPO frequency and HR follows an approximately exponential decay, with a slight indication of late saturation at higher QPO values. To study

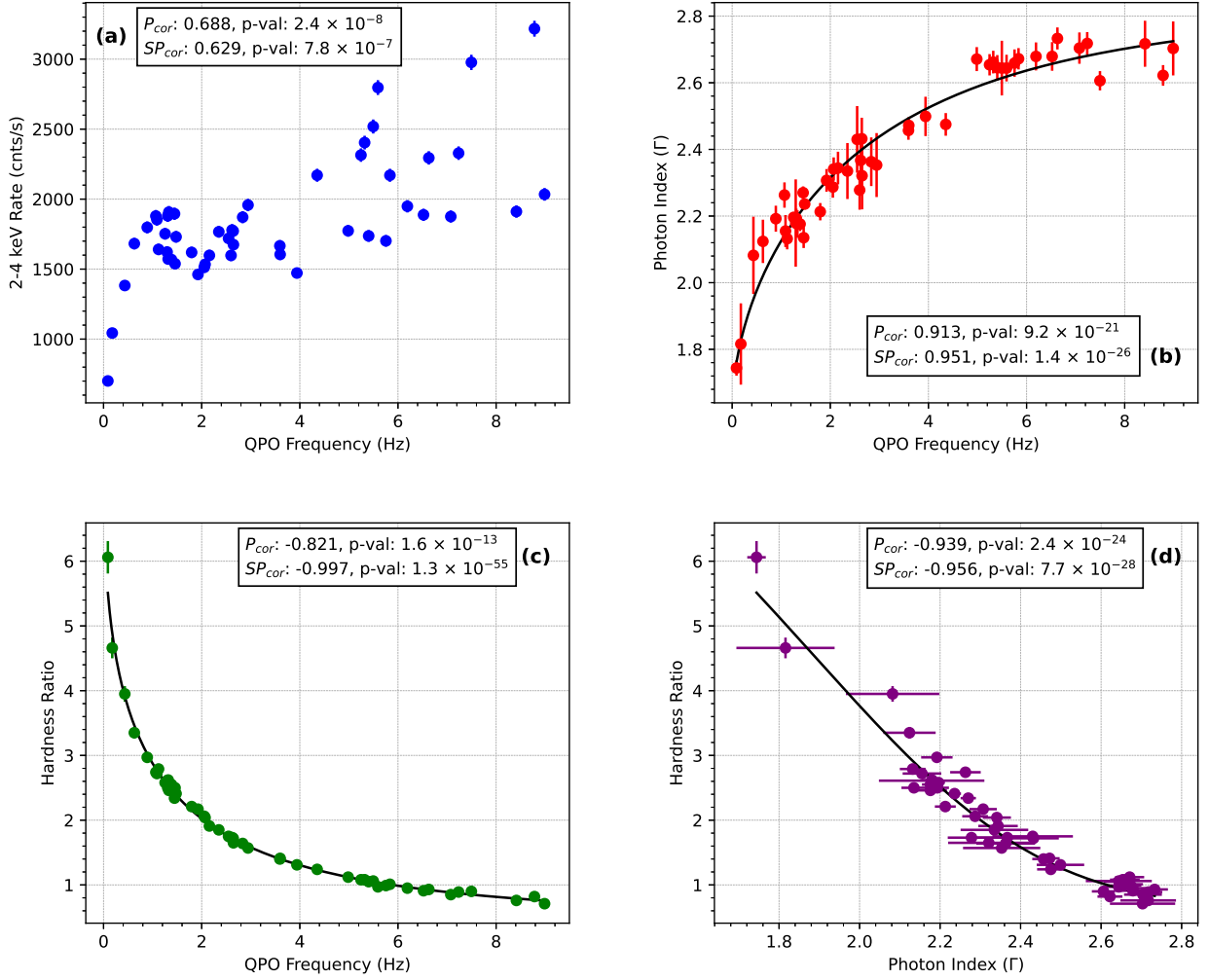


Figure 2. The variation of QPO frequency (ν_{QPO}) with (a) Soft X-ray (SXR; 2–4 keV) count rate, (b) photon index (Γ), and (c) Hardness ratio (HR), defined as the ratio of Hard X-ray (HXR; 2–150 keV) to SXR rates is shown. In (d), the variation of HR with Γ is presented. Pearson and Spearman rank correlation coefficients, i.e., P_{cor} and SR_{cor} , along with their p-values, are provided in the insets. The results indicate strong positive correlations of ν_{QPO} with SXR and Γ , whereas HR exhibits strong negative correlations with both ν_{QPO} and Γ . The ν_{QPO} - Γ positive correlation is fitted with scaling Eq. (6), and the Ed. (8) is used to fit negative correlations of HR with both ν_{QPO} and Γ (solid curves).

the relationship between ν_{QPO} and HR, we modified the scaling equation (6) by changing the sign between two factors on the right-hand side of the correlation formula. The modified equation is given by:

$$f(x) = A + D B \ln \left[\exp \left(\frac{1 - (x/x_{tr})^\beta}{D} \right) + 1 \right], \quad (8)$$

where x represents ν_{QPO} , and $f(x)$ corresponds to the calculated HR.

A strong anti-correlation trend between ν_{QPO} and HR is well fitted by the above Eq. (8), yielding a reduced χ^2 value of 1.01. The best-fit parameters with fixed $D=1$ are found to be: $A = 0.45 \pm 0.07$, $B = 5.57 \pm 0.53$, $\nu_{tr} = 0.31 \pm 0.08$, and $\beta = 0.40 \pm 0.04$. In Fig. 2(c), ν_{QPO} -HR data points (green) along with the model-fitted curve (solid black) are shown.

While studying the correlation between HR and the photon index (Γ), we found a strong anti-correlation between them. The Pearson and Spearman rank correlation coefficients are obtained as $P_{cor} = -0.939$ (with a p-value of 2.4×10^{-24}) and $SR_{cor} = -0.956$ (with a p-value of 7.7×10^{-28}). The variation of Γ vs. HR is also well fitted by Eq. (8) (see Fig. 2d). The best-fit parameters with $D=1$ are found to be: $A = 0.64 \pm 0.05$, $B = 6.82 \pm 0.90$, $\Gamma_{tr} = 1.77 \pm 0.07$, and $\beta = 3.48 \pm 0.35$. In Fig. 2(d), Γ -HR data points (purple) along with the model-fitted curve (solid black) are shown.

4.6. POS model fitted QPO evolution

The propagating oscillatory shock (POS) model is the time-varying form of the shock oscillation model (SOM), which explains the origin of QPOs due to the oscillation of the shock, i.e., the outer radius of the hot Compton

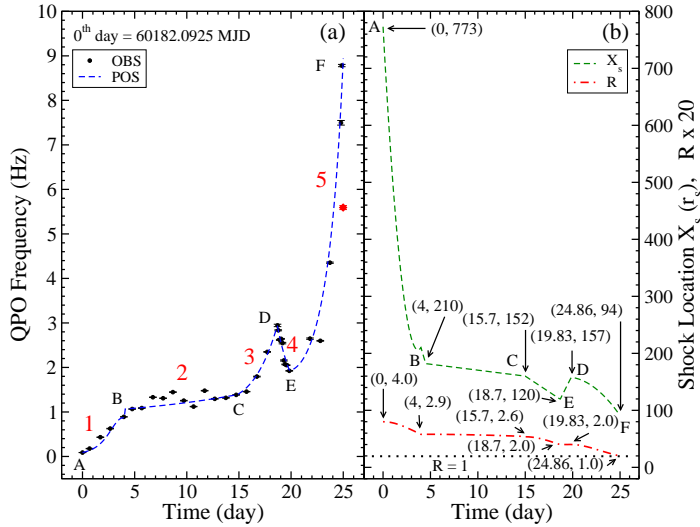


Figure 3. (a) Variations of the observed QPO frequencies with time (in day) from shaded parts (1-5) of Fig. 1, in the rising phase of the outburst with the fitted POS model (dotted curve) are shown. (b) Variation of the shock location (in Schwarzschild radius r_s) and shock compression ratio (R) are shown. Note, two diamonds points (online red) from shaded part 6 of Fig. 1 are not included in our model fitting, because the shock already achieved its weakest strength with $R = 1$ earlier on 2023 Sep. 19 (MJD=60206.28).

cloud or CENBOL. Thus, the oscillation of the shock corresponds to the oscillatory variation in the size of Compton cloud. During the rising phase of transient BHCs, the oscillating shock is found to move inward due to an increase in the rate of Keplerian disk matter. According to SOM, $\nu_{QPO} \sim X_s^{-3/2}$. As the shock moves inward, an increase in QPO frequencies is observed during the rising phase of an outburst. In the declining phase, the oscillating shock is found to move outward due to a rapid decrease in the rate of Keplerian disk matter. Consequently, in this phase, a monotonic decrease in QPO frequencies is observed over time.

This model has been used to study the evolution of QPOs during the rising and/or declining phases of outbursts in several sources, including GRO J1655-40 (Chakrabarti et al. 2005, 2008), GX 339-4 (Debnath et al. 2010, Nandi et al. 2012), H 1743-322 (Debnath et al. 2013), and XTE J1550-564 (Chakrabarti et al. 2009). The model fit provides the instantaneous location, strength, and velocity of the shock. Iyer et al. (2015) used this model to estimate the mass of the BHC IGR J17091-3624. These studies motivated us to investigate the evolution of QPO frequencies during the rising phase of Swift J1727.8-1613 using the POS model.

The evolving QPOs in parts (1-5) of the rising phase of the outburst of Swift J1727.8-1613 are fitted with the POS model (see Fig. 3). Except in part 4, the shock is found to move inward with decreasing strength.

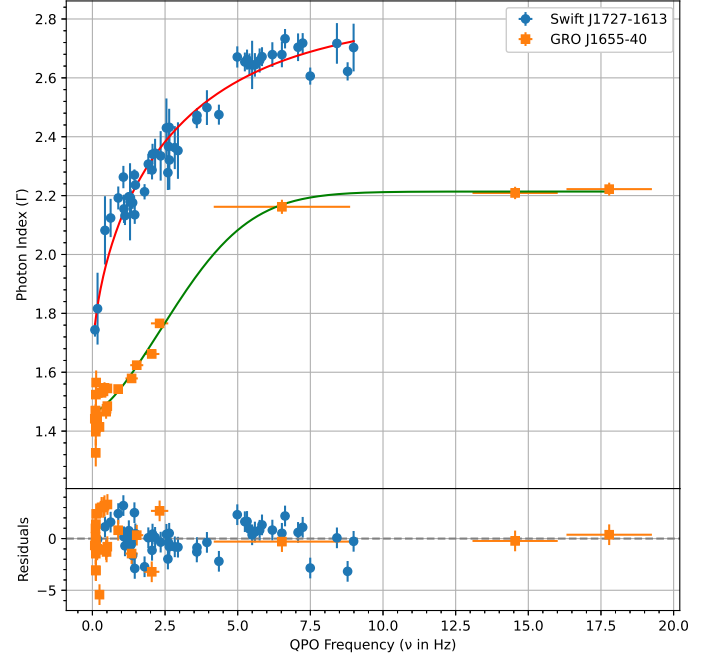


Figure 4. Photon index (Γ) vs. QPO frequency (ν_{QPO}) correlation scaling for the estimation of the mass of BHC Swift J1727.8-1613 using GRO J1655-40 as the known ($M_{BH} = 6.3 \pm 0.5 M_{\odot}$) reference source. Using model (Eq. 6) fitted ν_{tr} values of GRO J1655-40 ($\nu_{tr,J1655} = 2.82 \pm 0.09$) and Swift J1727.8-1613 ($\nu_{tr,J1727} = 1.31 \pm 0.14$), mass of the unknown BHC Swift J1727.8-1613 is estimated to be $13.54 \pm 1.87 M_{\odot}$. For GRO J1655-40, ν_{QPO} and Γ values are adopted from the rising phase data of 2005 outburst (see, Chakrabarti et al. 2008, Debnath et al. 2008).

Over ~ 25 days of the evolving phase, the shock location X_s decreases from $\sim 773r_s$ to $94r_s$, accompanied by a change in the compression ratio from its stronger ($R = 4$) to its weakest ($R = 1$) possible value. In Fig. 3, letters A-F denote the start, end, and transition days of different phases of QPO evolution. The shock is found to move inward rapidly in part 1, whereas in part 5, the shock weakens at a faster rate.

From the POS model fit of the QPO frequency evolution, the mass of the BHC Swift J1727.8-1613 is estimated to be $13.34 \pm 0.02 M_{\odot}$. To confirm this estimated mass, we applied the scaling method as defined in §2.2.

4.7. Mass Estimation From $\nu_{QPO} - \Gamma$ Scaling Method

According to §5.1 of Shakura & Sunyaev (1973), all characteristic dynamical timescales in accreting matter onto a compact object are determined by the mass of the object. The low-frequency QPO is also found to be inversely proportional to the mass of the black hole (BH). Therefore, one can scale the mass of the BH using the observed QPO frequency. Various methods for mass estimation based on low- and high-frequency QPOs have been proposed. Shaposhnikov & Titarchuk (2009) intro-

duced a more generalized method for mass scaling of an unknown source using a reference source with a known mass. The details of this method are already discussed in §2.2.

Here, we used the rising phase data of the QPO frequency and photon index (adopted from Chakrabarti et al. 2009 and Debnath et al. 2008) from the 2005 outburst of GRO J1655-40 as the reference source’s data. GRO J1655-40 is chosen as the reference since it exhibits a similar variation of $\nu - \Gamma$ as the target source Swift J1727.8-1613, and its mass is well known from dynamical methods (Greene et al. 2001). The Swift J1727.8-1613 photon index is obtained from spectral fitting in a broad energy range of 2 – 150 keV *Insight-HXMT* data. For spectral fit, we use the combined model: $constant \times tbabs(diskbb + pexrav)$. The best-fitted spectra using the above combined model provide photon index values, which are used here to study the $\nu - \Gamma$ correlation as well as mass scaling using Shaposhnikov & Titarchuk (2009) method.

The QPO evolution during the entire rising phases of both the unknown source Swift J1727.8-1613 (current 2023-24 outburst) and the reference source GRO J1655-40 (2005 outburst) is fitted with the $\nu - \Gamma$ correlation formula as defined in Eq. 6 (see, Fig. 4). While fitting, we use a fixed value of $D(=1)$. The set of model-fitted parameters: A , B , ν_{tr} , and β are obtained for both sources. For Swift J1727.8-1613, the model-fitted values are as follows: $A : 2.83 \pm 0.08$, $B : 0.91 \pm 0.10$, $\nu_{tr} : 1.31 \pm 0.14$, $\beta : 0.59 \pm 0.08$. For the reference source GRO J1655-40, the corresponding values are: $A : 2.21 \pm 0.01$, $B : 0.57 \pm 0.01$, $\nu_{tr} : 2.82 \pm 0.09$, $\beta : 1.82 \pm 0.09$. Using the scaling formula in Eq. 7 and the mass of the reference source GRO J1655-40 as $6.3 \pm 0.5 M_{\odot}$, we estimate the mass of the newly discovered Galactic transient black hole Swift J1727.8-1613 to be $13.54 \pm 1.87 M_{\odot}$. This value is in good agreement with the mass estimated using the POS model fit.

5. DISCUSSION AND CONCLUDING REMARKS

The discovery outburst of the Galactic transient BHC Swift J1727.8-1613 was first detected on 2023 Aug 24 (MJD = 60180), and it continued for the next ~ 10 months. In this *paper*, we present a detailed study of the outburst profiles, hardness ratios, and low-frequency QPOs during the rising phase (2023 Aug 25 to Oct 05; MJD = 60181.42-60222.20) of the outburst using broadband X-ray data from the *Insight-HXMT* instruments in the 2 – 150 keV energy range.

The daily variations in X-ray intensities in the soft (2 – 4 keV, SXR), hard (4 – 150 keV, HXR), and total (2 – 150 keV, TXR) energy bands show two distinct stages. In stage-I (up to 2023 Sep 13; MJD = 60200.12), TXR followed the HXR trend, while in stage-II (from 2023 Sep 13 to Oct 05; MJD = 60200.12-60222.20), TXR followed the SXR trend. From a physical perspective, we can infer that in stage-I, sub-Keplerian halo mat-

ter dominated, while in stage-II, Keplerian disk matter became dominant. Initially, both SXR and HXR rates increased and peaked on two different dates. The time gap between the HXR peak (MJD = 60184.07) and the SXR peak (MJD = 60186.19) allows us to estimate the viscous timescale of Swift J1727.8-1613 during its discovery outburst as ~ 2.12 days. Except for the initial and late rise in stage-I, the SXR rate remains roughly constant, indicating a steady supply of Keplerian matter from the pile-up radius. Subsequently, in stage-II, SXR exhibits multiple peaks, suggesting an uneven supply of disk matter. At the beginning of stage-II, the SXR rate declines sharply, indicating a sudden decrease in viscosity. On the other hand, in the post peak dates, the HXR rate decreases monotonically, except for two instances: in the middle of stage-I and at the beginning of stage-II.

Based on the evolution of QPO frequencies, we classify the rising phase of the outburst into six parts. Parts (1-5) are termed the “evolving phase”, while part 6 is categorized as the “non-evolving/sporadic phase”. QPO frequencies increase during parts 1-3 and 5, whereas in part 4, they decrease over time. During part 4, we observe a sharp rise in HR due to the increasing HXR trend and the simultaneous decreasing trend of SXR. From the evolution of QPOs and HRs in parts 1-3 and 5, we infer that the oscillating shock responsible for generating the observed LFQPOs moves inward due to the increasing cooling rate, as indicated by the relative increase in SXR over time. This also suggests that the size of the hot Compton cloud, which serves as the reservoir of hot electrons that upscatter thermal photons from the Keplerian disk, reduces over time. However, in part 4, the shock moves outward, leading to an increasing Compton cloud size due to a reduced cooling rate, as evidenced by the increase in HXR and the decrease in SXR.

Throughout the entire rising phase, the observed QPO frequencies vary in a manner similar to SXR and photon index, and inversely to HR (Fig. 1). To confirm these trends statistically, we perform correlation studies using the Pearson and Spearman rank methods (see, Fig. 2). Both correlation methods show a strong positive correlation between QPO frequency and SXR, as well as photon index, and a strong negative correlation between HR and QPO frequency as well as HR with photon index. The correlation and anti-correlation trends of QPO frequency, photon index, and HR values, are further fitted using the relations defined in Eqs. 6 and 8.

We further study the evolution of QPO frequencies during the evolving phase (parts 1-5) using the propagating oscillatory shock (POS) model. The instantaneous location and strength of the shock, responsible for generating the observed LFQPOs are obtained from the model fit. During the entire evolving phase of ~ 25 days, the shock moves inward from $X_s = 773r_s$ to $94r_s$ while weakening in strength. The shock compression ratio R (inverse of the strength β_s) decreases from its stronger value ($R = 4$) to its weakest possible value ($R = 1$). In

part 4, which lasts ~ 1.2 days, the shock recedes from $119r_s$ to $157r_s$. Additionally, we observe that in part 1, the shock moves rapidly inward, whereas in part 5, the shock weakens at a faster rate. The best-fitted POS model for the QPO frequency evolution also allows us to infer the probable mass of the BHC Swift J1727.8-1613 as $13.34 \pm 0.02 M_\odot$, since the mass of the BH is a crucial parameter in the POS model (see §2.1).

To verify the mass obtained from the POS model, we employ an independent $\nu - \Gamma$ scaling method. Here, we use the 2005 rising phase data of the well-known transient BH GRO J1655-40 as the reference source to scale the mass of the unknown BHC Swift J1727.8-1613. The QPO frequency vs. photon index evolution of both sources is fitted with Eq. 6 to determine the scaling model parameters. Using the best-fitted transition frequencies (ν_{tr}) of the two sources and the dynamically measured mass of the reference source, we estimate the mass of Swift J1727.8-1613 as $13.54 \pm 1.87 M_\odot$. By combining the POS model and $\nu - \Gamma$ scaling methods, we infer the probable mass of the newly discovered Galactic transient BHC Swift J1727.8-1613 as $13.54 \pm 1.87 M_\odot$. This result roughly agrees with Debnath et al. (2024) estimated source mass ($10.2 \pm 0.4 M_\odot$) from the spectral analysis with the TCAF model.

A brief summary of our findings in this *paper* is as follows:

- i) The rising phase of the outburst exhibits two distinctly different stages based on the variations in soft (SXR; 2-4 keV), hard (HXR; 4-150 keV), and total (TXR; 2-150 keV) X-ray rates. In stage-I, TXR correlates with HXR, while in stage-II, TXR correlates with SXR.

- ii) Strong signatures of type-C LFQPOs are observed throughout the rising phase. We further classify the rising phase of the outburst into six parts based on the nature of the evolution of ν_{QPO} . In parts 1-3 and 5 of the evolving phase, the shock is found to move inward as ν_{QPO} increases, whereas in part 4, a receding shock is observed as ν_{QPO} decreases. No clear trend of ν_{QPO} is seen in part 6.
- iii) A strong positive correlation of ν_{QPO} with SXR as well as the photon index is noticed.
- iv) A strong negative or anti-correlation of HR with ν_{QPO} as well as the photon index is observed.
- v) The POS model fit of ν_{QPO} during the evolving phase (parts 1-5) allows us to determine the instantaneous location, strength, and velocity of the shock. It also provides the most probable mass of the BHC as $13.34 \pm 0.02 M_\odot$.
- vi) The $\nu - \Gamma$ scaling method enables us to estimate the mass of the newly discovered BHC Swift J1727.8-1613 as $13.54 \pm 1.87 M_\odot$, using GRO J1655-40 as the reference source.

ACKNOWLEDGEMENTS

This work made use of archival data of *Insight*-HXMT, a mission satellite project of China National Space Administration (CNSA) and Chinese Academy of Sciences (CAS). D.D. acknowledge the visiting research grant of National Tsing Hua University, Taiwan (NSTC NSTC 113-2811-M-007-010). H.-K. C. is supported by NSTC of Taiwan under grant NSTC 113-2112-M-007-020. S.K.N. acknowledges support from the visiting research grant of National Tsing Hua University.

REFERENCES

- Belloni, T., Homan, J., Casella, P., et al., 2005, *A&A*, 440, 207
- Bhowmick, R., Debnath, D., Chatterjee, K., et al., 2021, *ApJ*, 910, 138
- Casella, P., Belloni, T., & Stella, L., 2005, *ApJ*, 629, 403
- Chakrabarti, S. K. 1990, *Theory of Transonic Astrophysical Flows*. Edited by CHAKRABARTI SANDIP K. Published by World Scientific Publishing Co. Pte. Ltd., ISBN #9789814439220. doi:10.1142/1091
- Chakrabarti, S. K. & Titarchuk, L. G., 1995, *ApJ*, 455, 623
- Chakrabarti, S.K., Nandi, A., Debnath, D. Sarkar, R. & Datta, B.G., 2005, *Ind. J. Phys.*, 78B, 1
- Chakrabarti, S.K., Debnath, D., Nandi, A., Pal, P. S., 2008, *A&A* 489, L41
- Chakrabarti, S. K., Dutta, B. G., Pal, P. S., 2009, *MNRAS*, 394, 1463
- Chakrabarti S. K., Mondal, S. Debnath, D., 2015, *MNRAS*, 452, 3451
- Chakrabarti, S. K., Debnath, D., Nagarkoti, S., 2019, *AdSpR*, 63, 3749
- Chatterjee, K., Debnath D., Bhowmick, R., et al., 2022, *MNRAS*, 510, 1128
- Debnath, D., Chakrabarti, S.K., Nandi, A., & Mandal, S., 2008, *BASI*, 36, 151
- Debnath, D., Chakrabarti, S.K., & Nandi, A., 2013, *AdSpR*, 52, 2143
- Debnath, D., Mondal, S., & Chakrabarti, S.K., 2015, *MNRAS*, 447, 1984
- Debnath, D., Jana, A., Chakrabarti, S. K., Chatterjee, D., & Mondal, S., 2017, *ApJ*, 850, 52
- Debnath, D., Chatterjee, K., Chatterjee, D., et al., 2021, *MNRAS*, 504, 4242

- Debnath, D., Nath, S., Chatterjee, D., Chatterjee, K., Chang, H- K., 2024, *ApJ*, 975, 194
- Ebisawa, K., Titarchuk, L., Chakrabarti, S. K., 1996, *PASJ*, 48, 59
- Greene, J., Bailyn, C. D., Orosz, J. A., 2001, *ApJ*, 554, 1290
- Ingram, A., Done, C., 2011, *MNRAS*, 415, 2323
- Ingram, A., Bollemeijer, N., Veledina, A, et al., 2024, *ApJ*, 968, 76
- Iyer, N., Nandi, A., & Mandal, S., 2015, *ApJ*, 807, 108
- Jana, A., Chakrabarti, S. K., & Debnath, D., 2017, *ApJ*, 850, 91
- Kennea, J. A. & Swift Team, 2023, *GCN*, 34540, 1
- Molteni D., Sponholz H., Chakrabarti S. K., 1996, *ApJ*, 457, 805
- Motta, S. E., Muñoz-Darias, T., Sanna, A., 2014, *MNRAS*, 439, L65
- Nandi, A., Debnath, D., & Mandal, S., et al., 2012, *A&A*, 542, 56
- Nandi, A., Das, S., Majumder, S., et al., 2024, *MNRAS*, 531, 1149
- Peng, J- Q., Zhang, S., Shui, Q- C., et al., 2024, *ApJ*, 960, L17
- Podgorný, J.; Svoboda, J.; Dovčiak, M., et al., 2024, *A&A*, 686, L12
- Remillard, R. A., & McClintock, J. E., 2006, *ARA&A*, 44, 49
- Russell, D. M., Bramich, D. M., Lewis, F., et al., 2018, *Astron. Nach.*, 340, 278
- Ryu, D., Chakrabarti, S. K., Molteni, D., 1997, *ApJ*, 474, 378
- Rodriguez, J., Varnière, P., Tagger, M., Durouchoux, P., 2002, *A&A*, 387, 487
- Sánchez, D., Torres, M. A. P., Casares, J., et al. 2025, *A&A*, 693, A129
- Shakura, N. I., & Sunyaev, R. A. 1973, *A&A*, 24, 337
- Shaposhnikov, N., & Titarchuk, L. 2007, *ApJ*, 663, 445
- Shaposhnikov, N., & Titarchuk, L. 2009, *ApJ*, 699, 453
- Stella L., Vietri M., 1999, *NuPhS*, 69, 135
- Tagger M., Pellat R., 1999, *A&A*, 349, 1003
- Titarchuk L., Lapidus I., Muslimov A., 1998, *ApJ*, 499, 315
- Titarchuk L., Osherovich V., 2000, *ApJ*, 542, L111
- Titarchuk, L. G., & Fiorito, R. 2004, *ApJ*, 612, 988
- Trudolyubov S., Churazov E., Gilfanov M., 1999, *A&A*, 351, L15
- Zdziarski, A. A., & Magdziarz, P., 1995, *MNRAS*, 273, 837
- Veledina, A., Muleri, F., Dovčiak, M., et al., 2023, *ApJ*, 958, L16
- Mereminskiy, I., Lutovinov, A., Molkov, S., et al., 2024, *MNRAS*, 531, 4893
- Zhu, H., & Wang, W., 2024, *ApJ*, 968, 106